Effect of environmental drivers on the spatiotemporal distribution of mackerel at age in the Nordic Seas during 2010-2020

Authors: Ono, K[1]., Katara, I.[2,3], Eliasen, S.K[4]., Broms, C. [1], Campbell, A.[6], dos Santos Schmidt[5], T.C., Egan[6], A., Jacobsen, J.A.[4], Jansen, T.[7,8], Mackinson, S.[9], Mousing, E.A. [1], Nash, R.D.M.[2]., Nikolioudakis, N. [1], Nnanatu, C.[2,10], Hølleland, S.N[11], Nøttestad, L.[1], Singh, W.[5], Slotte, A.[1], Wieland, K.[8], and Olafsdottir, A.H.[5]

Affiliation:

1 Institute of Marine Research (IMR), Nordnesgaten 50, 5005 Bergen, Norway.

2 Centre for Environment, Fisheries and Aquaculture Science (Cefas), Pakefield Road, Lowestoft, Suffolk, NR33 0HT, UK.

3 International Whaling Commission (IWC), The Red House, 135 Station Road, Impington, Cambridge, CB24 9NP, UK.

4 Faroe Marine Research Institute (FAMRI), Nóatún 1, FO-100 Tórshavn, Faroe Islands.

5 Marine and Freshwater Research Institute, Fornubúðir 5, IS-220 Hafnarfjörður, Iceland.

6 Marine Institute, Rinville, Oranmore, Co Galway, Ireland.

7 GINR (Greenland Institute of Natural Resources), Kivioq 2, PO Box 570, 3900 Nuuk, Greenland.

8 DTU AQUA (National Institute of Aquatic Resources), Kemitorvet, 2800 Kgs. Lyngby, Denmark.

9 Scottish Pelagic Fishermen's Association, Heritage House, Shore Street, Fraserburgh, Aberdeenshire, AB43 9BP, UK.

10 WorldPop Research Group, School of Geography and Environmental Science, University of Southampton, SO17 1BJ, Highfield Campus, Southampton, UK

11 Department of Business and Management Science, Norwegian School of Economics, Helleveien 30, 5045 Bergen, Norway

Key words – Northeast Atlantic mackerel, *Scomber scombrus*, joint spatio-temporal model, species distribution, year-class, migration, SST

1. Abstract

A joint spatio-temporal distribution model of mackerel (ages 3 to 10) was developed to investigate the age-based responses of mackerel to three environmental drivers: sea surface temperature (SST), mixed layer depth, and chlorophyll-a concentration during the summer months 2010-2020 in the Nordic Seas. The study showed that SST was the most important variable amongst the one tested and had the strongest impact on the distribution of the younger age classes (3-5) which had a narrower range of favourable SST and a stronger aversion to cold temperature than older individuals. Consequently, the impact of SST differed regionally; in the polar front regions, SST explained up to 61% of the variability in the observed density of young individuals where Arctic water masses likely acted as a barrier to these young individuals. That said, part of it could be

confounded with the limited migration capability of young mackerels which could not reach the furthest frontal regions. In warmer southern waters, the same environmental variables had less explanatory power for mackerel of all ages. Individuals in the south were likely not constrained by temperature and perhaps more influenced by other variables such as food availability or ocean current (throughout their migration path), for which appropriate data are lacking. Moreover, the model showed that older mackerel were distributed more to the north and west and their migration pattern changed when the 2013 year-class no longer migrated to the west compared to previous year-classes. Additionally, all year classes started migrating more eastward from summer 2018.

2. Introduction

The annual geographical distribution of migratory pelagic fish stocks is often dynamic. The area occupied during the seasonal migration cycle can remain stable for years (Carscadden *et al.*, 2013), change gradually (Dragesund *et al.*, 1997) or abruptly (Frank *et al.*, 1996; Roy *et al.*, 2007). Distributional changes can occur in some or all parts of the seasonal migration cycle of feeding, overwintering, and spawning (Frank *et al.*, 1996). Factors that drive such changes include abiotic (Frank *et al*., 1996) and biotic environmental conditions (Kvamme *et al.*, 2003; Pacariz *et al.*, 2016), numerical dominance of some year-classes (Huse *et al.*, 2002), learning (Corten, 2002), age-specific response (Ono *et al.*, 2022), and stock size (Barange *et al.*, 2009; Olafsdottir *et al.*, 2019).

Northeast Atlantic mackerel (*Scomber scombrus,* Linnaeus, 1758) is a temperate pelagic fish which migrates seasonally between spawning, feeding and overwintering areas (Trenkel *et al.*, 2014). Most spawning occurs in the Bay of Biscay, and west of Ireland and Scotland, progressing northward between March and May. After spawning, much of the mature part of the stock migrates northwards into the Norwegian Sea and adjacent areas for feeding during the summer. The central and eastern parts of the Norwegian Sea are influenced by relatively warm surface currents of Atlantic origin, in contrast to the western region, which is separated from the central part by the Jan Mayen Front and is influenced by relatively cold currents of Arctic origin (Figure 1a; Read and Pollard, 1992; Blindheim and Østerhus, 2005). Mackerel prefers temperatures in the range of 8 – 13 °C but can tolerate waters as cold as 5 °C (Nikolioudakis *et al.*, 2019; Olafsdottir *et al.*, 2019). During the summer months (late June to late September), the vertical distribution of mackerel in the Norwegian Sea is dictated by surface temperature as it is only the upper mixed layer which is sufficiently warm. In the southern parts of the summer feeding area - i.e., the southeastern Norwegian Sea and northern North Sea, on the Iceland-Faroe Ridge and south of Iceland - the vertical distribution of mackerel is not limited to the uppermost layer since temperatures there are slightly higher than in the north (Nøttestad et al. 2015, 2016a, 2017, 2019, Olafsdottir *et al.* 2018, ICES 2020, 2021). The horizontal distribution of mackerel within the summer feeding area is also related to size (Nøttestad *et al.*, 1999) and age (Ono *et al.*, 2022). Older and larger mackerel migrate further northward and westward from their spawning areas during the summer feeding migration whereas the distribution of smaller and younger fish is generally limited to the central and eastern Norwegian Sea (Nøttestad *et al.,* 2015, 2016a, 2017, 2019, Olafsdottir *et al.,* 2018, ICES 2020, 2021, Ono *et al.,* 2022).

Over the last two decades, the summer feeding area of mackerel has both expanded and contracted (Figure 1b) (Astthorsson *et al.*, 2012; Utne *et al.*, 2012; Olafsdottir *et al.,* 2019; ICES, 2020). Prior to the expansion, the feeding area was limited to the central Norwegian Sea (Utne *et al.*, 2012). In the mid-2000s, the mackerel distribution expanded westward, first into Icelandic waters (Astthorsson *et al.*, 2012) and then into Greenlandic waters (Nøttestad *et al.*, 2016b; Jansen *et al.*, 2016). The widest

distribution was observed in summer 2014 when substantial amounts of fish were encountered at 42.5°W and with a single mackerel found as far west as 51° W (Jansen *et al.*, 2016). In 2017, a reduction in the distributional range from Greenlandic waters began, with a further retraction to Icelandic waters by 2019, and then to the east coast of Iceland by 2020. During the same period, the mackerel distribution in the Norwegian Sea expanded northward towards Svalbard with the northern boundary occurring close to 77° N in the summer of 2020 (ICES, 2020).

The distribution and density of the mackerel stock during the summer feeding season has been studied since 2007 using data collected during the International Ecosystem Summer Survey in Nordic Seas (IESSNS) (Nøttestad *et al.*, 2016b). Several modelling frameworks, including statistical and mechanistic, have been developed to identify the drivers of mackerel's summer distribution. Nikolioudakis et al. (2019) developed a Bayesian hierarchical spatiotemporal model and Olafsdottir et al. (2019) a generalized additive model to find statistical relationships between local age-aggregated mackerel abundance (or presence) and environmental covariates. Boyd et al. (2020) developed a bioenergetic individual-based model that uses our understanding of the mechanisms driving mackerel migration but without fitting to data. Both approaches suggested that temperature and prey abundance indicators positively impacted mackerel presence and density.

In the current study, we extended previous spatiotemporal modelling work on mackerel (e.g Nikolioudakis et al. (2019) and Olafsdottir et al. (2019)) and jointly modelled the distribution of mackerel between ages 3 to 10 by considering the correlation in mackerel density in space, time, and age as well as the effect of the available key environmental drivers. The current paper has one principal objective, to explore the impact of sea surface temperature, mixed layer depth, and chlorophyll-a concentration (as an indicator of productive waters, thus food availability) on the summer distribution of mackerel at age. The hypothesis tested is that within the recorded ranges of the explored environmental covariates, warmer temperatures, greater mixed layer depth, and higher chlorophyll-a concentration result in higher mackerel density but with a differential response by age. Younger mackerel are expected have a higher thermal preference than older individuals due to physiological constraints (McCauley and Huggins, 1979; Lafrance et al., 2005; Freitas et al. 2010; Morita et al. 2010). Greater mixed layer depth would allow a greater volume of the water column to be inhabited by mackerel, thus allowing higher abundance, irrespective of mackerel age. Finally, a higher chlorophyll-a concentration would suggest higher food availability which would attract more mackerel to the area.

3. Material and Methods

To study the spatio-temporal changes in mackerel summer distribution, disaggregated by age, from 2010 to 2020, we combined age-disaggregated mackerel catch data from the July IESSNS survey (Supplementary Figure S1) with environmental data derived via remote sensing and oceanographic models (Table 1. Supplementary Figure S2-4). The analysis was limited to this period for two reasons: age and year-class included in the time series must be continuous for the developed model (no more than 2 years apart) and from 2020 onwards environmental data was unavailable at the time of the analyses. The analysis is limited to mackerel aged 3 to 10 years, as younger individuals are mostly distributed south of the IESSNS survey area (Jansen *et al.*, 2015).

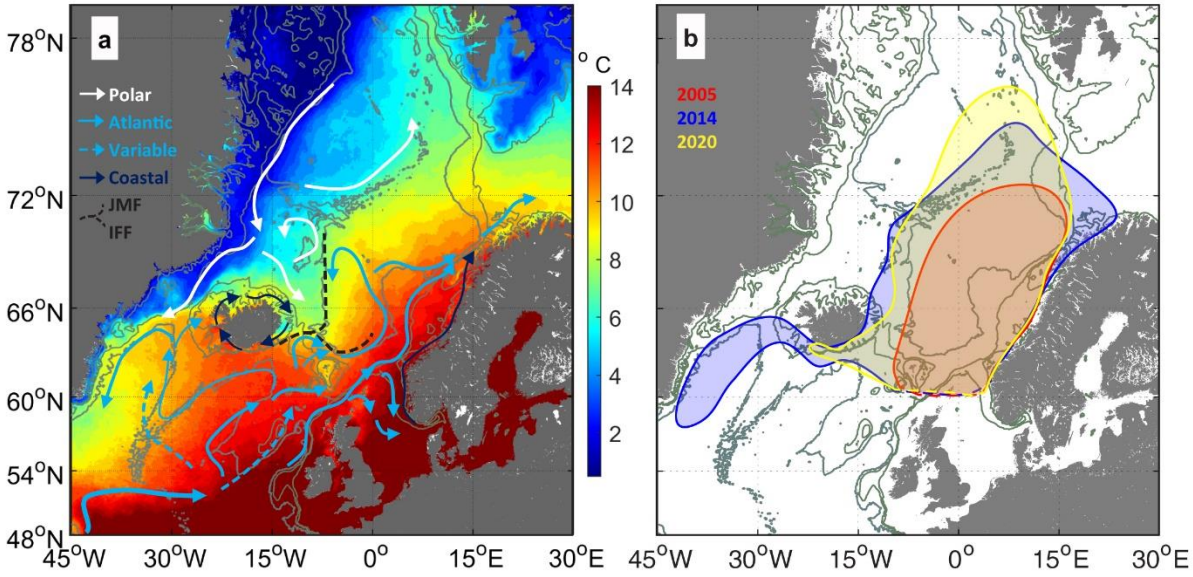

Figure 1. a) Main features of the near-surface circulation in the Northeast Atlantic and the Nordic Seas. Light blue arrows indicate relatively warm water masses with dashed arrows indicating variable currents. Dark blue arrows indicate coastal currents and white indicate relatively cold-water masses. Modified from Hansen & Østerhus, 2000; Turell, 1995; Stefánsson & Ólafsson, 1991. Overlaid is the remotely sensed average sea surface temperature (SST) for July from 2010 to 2020 (from NASA Goddard Space Flight Centre, Ocean Ecology Laboratory, Ocean Biology Processing Group), with 200 m, 500 m, and 2000 m depth contours shown in grey and the Jan Mayen Front (JMF) and the Iceland-Faroe Front (IFF) shown with black dashed lines. b) Mackerel distribution in the Norwegian Sea and adjacent areas during summer, before the expansion (2005 - red, adjusted from Utne et al., 2012), when it was at its maximum (2014 - blue, based on IESSNS survey) and the last study year (2020 - yellow, based on IESSNS survey). The distribution illustrated in the figure is restricted to the study area and, as such, does not cover the eastern areas south of 60 °N (dotted lines).

3.1. Environmental data

The variables tested were Sea Surface Temperature (SST), the concentration of chlorophyll-a (CHL), and mixed layer depth (OMLT) (Table 1). All were derived on a monthly time scale for July (the survey month) and extracted for each survey point using bilinear interpolation from the source data. Raster stacks of all parameters at an annual time step were also produced at a spatial resolution of 5.5 km (by bilinear interpolation) and used for model predictions (Supplementary Figure S2-4).

Table 1. Source of environmental parameters with a short description and spatial resolution.

Variable (abbreviation)	Source	Spatial resolution

Global Ocean OSTIA Sea Surface Temperature (SST)	copernicus.eu[1,2] product identifier: SST_GLO_SST_L4_NRT_OBSERVATIONS_010_001 level 4 processed satellite observations original data: Met Office (UK)	0.05°
Mass concentration of chlorophyll a in sea water (CHL)	copernicus.eu[3] product identifier: OCEANCOLOUR_GLO_CHL_L4_REP_OBSERVATIONS_009_082 level 4 processed satellite observations	4 km
Mixed layer depth defined by sigma theta (OMLT)	copernicus.eu[4] product identifier: GLOBAL_MULTIYEAR_PHY_001_030 level 4 Global Ocean Physics Reanalysis product (numerical model)	0.083°

3.2. Biological data – mackerel IESSNS survey

IESSNS is approximately a month-long systematic surface trawl survey conducted between July and early August where the survey area is split into thirteen strata of unequal dimension (ICES 2022b, Figure 2). This study focuses on strata 1-12 (excluding stratum 8). The survey uses a swept-area method based on standardised surface trawling at predetermined locations using stratified random design with variable effort between strata (Nøttestad *et al.*, 2016b). The first survey was undertaken in July 2007 but since 2010 it was expanded considerably and conducted annually as an internationally coordinated survey (Nøttestad *et al.*, 2016b; ICES 2022a). Survey coverage approximately doubled from 1.7 million km^2 in 2007 to a peak of 3.1 million km^2 in 2014 to track the expanding mackerel distribution westward and northward (Nøttestad *et al.*, 2016b). Coverage has remained at a similar level since 2014 (ICES, 2020).

For each stratum, the survey starts at a random point and has a fixed distance between stations. Effort varies between strata and ranges from 30-90 NM between stations (ICES, 2022b). Each of the twelve strata is either categorized as permanent (strata 1, 2, 3, 5, 6, 7, 10 and 11) or dynamic (strata 4, 9, 12) (Figure 2). Permanent strata are fully covered every year while coverage in dynamic strata is limited by the extent of the mackerel distribution (ICES, 2022b). Dynamic boundaries in frontal regions (strata 4 and 9) are located where SST declines below 4-5°C and normally no mackerel or only a few individuals are caught (< 10 fish; personal communication A. Ólafsdóttir, cruise leader IESSNS Icelandic vessel, May 15th, 2024). For stratum 12, temperate Atlantic waters south of Iceland, survey transects run from north to south, and the dynamic southern boundary is located at the first station with no mackerel caught or only a few individuals (< 10 fish; personal communication A. Ólafsdóttir, cruise leader IESSNS Icelandic vessel, May 15th, 2024). Survey coverage has generally expanded westward and northward from 2010 to 2014 in response to expanding mackerel distribution (Nøttestad *et al.*, 2016a; 2010-2020 annual survey coverage) but remained similar between 2014-2020. In 2011, the survey coverage in the Norwegian Sea was limited to south of 71 °N (Nøttestad *et al.*, 2011).

[1] ftp://nrt.cmems-du.eu/Core/SST_GLO_SST_L4_NRT_OBSERVATIONS_010_001/METOFFICE-GLO-SST-L4-NRT-OBS-SST-MON-V2

[2] https://doi.org/10.48670/moi-00165

[3] https://resources.marine.copernicus.eu/product-detail/OCEANCOLOUR_GLO_CHL_L4_REP_OBSERVATIONS_009_082/INFORMATION

[4] https://doi.org/10.48670/moi-00021

At each station, a standardized surface haul is conducted where a standardised trawl is towed for 30 min at a target speed of 5 knots (2.6 m sec^{-1}) (ICES, 2022b). The realized recorded speed range was 3.3-5.9 knots (1.7-3.0 m sec^{-1}) (Nøttestad *et al.*, 2015, 2016a, 2017, 2019; Olafsdottir *et al.,* 2018; ICES, 2020, 2021). Floats are attached to the headline and to the wings, and kites on the top panel, to secure its position at the surface and aiming for a vertical trawl opening of 30-35 m. The recorded realized range of the vertical opening of the trawl was 17-52 m (Nøttestad *et al.,* 2015, 2016a, 2017, 2019; Olafsdottir *et al.,* 2018; ICES, 2020, 2021). The total catch is weighted, and species composition determined by sorting the whole catch or by taking a random sample. Next, the body weight (± 0.5 g) and length (from the tip of the snout to the upper lobe of the pinched caudal fin; ± 0.5 cm) of individuals from haphazard sub-sample of 10-100 are measured. From these sub-samples, 10-50 individuals are then randomly selected and aged. During 2010-2020, a total of 2838 stations were covered by the survey in strata 1-12 (see ICES 2022b for a complete description of the biological sampling process).

3.3. Calculations of mackerel biomass density

Mackerel biomass density *y* [kg km^{-2}], was calculated based on trawl data, i.e., tow-time, tow-speed, catch of each trawl haul, and the width of the trawls (Nøttestad *et al.*, 2015, 2016a, 2017, 2019, Olafsdottir et al. 2018, ICES 2020, 2021):

$$y = \frac{C}{W \cdot L} = \frac{C}{W \cdot t \cdot v} \qquad \textit{Eq 1}$$

where: *C* = Catch [kg], *W* = trawl width [km], *L* = distance sailed during haul [km], *t* = length of haul [hours] and *v* = speed during haul [km $hour^{-1}$].

Hereon, density will refer to the biomass density and not the density in number of fish. For each station, the aggregated density was allocated to different age groups, *a*, based on its proportion by weight (p_a) from the biological sample.

$$y_a = y \cdot p_a \qquad \textit{Eq 2}$$

For stations without mackerel (n=553), density at age *a*, y_a, was set to 0, thus the data was augmented properly. For stations with catch > 0 but without biological sampling (n=93), density at age was not calculated and the data were excluded from the model.

3.4. Modelling framework

We developed a multivariate spatio-temporal distribution model to analyse the age-based summer distribution of mackerel in the Nordic Seas between 2010-2020 and determine the contribution of selected environmental factors to the variability in modelled distribution. The model can be described as follows:

$$\mu_a(i) = \sum_{j=1}^{p} \beta_a(j) X(i,j) + w_a(v_i) + \varepsilon(s_i, t_i, a), \quad for\ a = 1, \ldots, A,\ i=1,\ldots,n, \qquad \textit{Eq 3}$$

$$w_a(v_i) \sim Gaussian\left(0, \sigma^2_{w,a}\right), \text{ for } a = 1, \ldots, A,\ i=1,\ldots,n, \qquad \textit{Eq 4}$$

where $\mu_a(i)$ is the expected mackerel density for station *i* (n stations in total) for age group *a* (from 1 to *A* groups), **X** is the (n x *p*) design matrix of covariates (e.g. the year effect (treated as factor), SST, CHL concentration, OMLT, stratum effect for non-spatial model) and β (*p* x *A*) is the matrix of

covariate effects to be estimated for each age group. The index *j* corresponds to the covariate number from 1 to *p*. $w_a(\mathrm{v_i})$ is the vessel random effect for vessel v_i and age group *a* that captures the difference in catchability associated with the vessel with variability $\sigma^2_{w,a}$ (kept the same across ages as it was almost identical across ages – see Supplementary Table S1 for details on parameter definitions and specifications). $\varepsilon(s_i, t_i, a)$ is the spatio-temporal random effect value for location s_i, time t_i (a total of *T* time steps), and age group *a* which is modelled using an INLA-inspired approach (Rue et al. 2009 – see more description below). Unlike other spatio-temporal models in the literature, the above model does not include a time-invariant spatial random effect. The latter is often interpreted as the underlying spatial productivity field, but this concept does not apply to a highly mobile species such as mackerel that shows large fluctuations in annual distributions. Moreover, extra flexibility was added to ε to capture the large variability in the joint space, time, and age mackerel dynamics. ε was modelled as a Gaussian process and considered the correlation over space and among age groups by year. This resembles other multi-categorical models available in the literature, such as VAST (Thorson, 2019):

$$\mathrm{vec}(\varepsilon(\cdot, t, \cdot)) \sim \mathrm{MVN}(0, \mathbf{R}_\mathrm{t} \otimes \mathbf{V}_\mathrm{t}), \quad \mathrm{t} = 1, \ldots., \mathrm{T}, \qquad \textit{Eq 5}$$

where vec denotes the vectorization-, or stacking, operator, $\mathbf{R}_\mathrm{t}$ is the covariance matrix among locations for year *t* that follows a Matérn process C_m, approximated by the stochastic partial differential equation approach of Lindgren *et al.* (2011). This approach involves discretizing the spatial domain into a 2D mesh (see Supplementary Figure S5 for the chosen mesh structure). Let M denote the set coordinates for the nodes in the mesh. Then

$$\mathbf{R}_\mathrm{t} = \{C_m(\|s_2 - s_1\| \mid \delta_t^2, \kappa_t)\}_{s_1, s_2 \in M}, \qquad \mathrm{t} = 1, \ldots., \mathrm{T}, \qquad \textit{Eq 6}$$

where δ_t^2 denotes the marginal variance and κ_t is the spatial scale parameter. To ensure identifiability of $\mathbf{V}_\mathrm{t}$, we set $\delta_t^2 = 1$ for all t. The spatial scale parameter $\kappa_t = \kappa$ is assumed to be identical between years i.e. the spatial correlation structure does not change between years (even when relaxing this assumption, κ_t was almost unchanged between years). Prior to all model fitting, coordinates were projected to EPSG:3035 to preserve distances. The extra flexibility came from the construction of the annual covariance in spatial distribution between age groups, $\mathbf{V}_\mathrm{t}$. Correlation between age groups is often assumed to depend on the age difference between groups (i.e. distance in age), similar to assuming a first-order autoregressive (AR1) structure in age. However, the correlation between mackerel age groups extensively changed by year during the study period and thus it did not follow an AR1-like correlation structure based on age difference (Supplementary Figure S6). Using an AR1 correlation in age for $\mathbf{V}_\mathrm{t}$ increased the Akaike Information Criterion (AIC) of the most parsimonious model (defined below) by almost 5000 units and estimated unrealistically high abundances for the youngest age groups during model testing. Consequently, $\mathbf{V}_\mathrm{t}$ was modelled in this study by using the annual empirical (from the data) correlation matrix between age groups, $\mathbf{E}_\mathrm{t}$, scaled up by a diagonal matrix $\boldsymbol{\lambda}$ where the diagonal entries are the marginal standard deviation for each age group, η_a (estimated by the model).

$$\boldsymbol{V}_t = \boldsymbol{\lambda}\, \boldsymbol{E}_t \boldsymbol{\lambda}. \qquad \textit{Eq 7}$$

Finally, the observed mackerel density $y_a(i)$ for age *a* and observation *i* was modelled using a Tweedie distribution with mean $\mu_a(i)$ (*Eq* 3), dispersion parameter τ_a and a power parameter θ_a:

$$y_a(i) \sim tweedie(\mu_a(i), \tau_a, \theta_a), \; a = 1, \ldots., A, \; i = 1, \ldots, n. \qquad \textit{Eq 8}$$

The Barrier approach proposed by Bakka *et al.* (2019) was used for all models presented in this study to account for physical barriers (e.g. Iceland and Norwegian coasts) in the ocean to reduce artificial correlation patterns across physical barriers.

The functional form of covariate effect was selected based on visual exploration of the relationship between the covariates and the density of mackerel in each age group (Zuur *et al.*, 2010, Supplementary Figure S7). All continuous variables were scaled before the analysis. Subsequently, variables were either modelled linearly or using thin-plate regression splines for non-linear pattern as implemented in the R *mgcv* package (Wood, 2003, 2011). The degree of smoothness was limited to 3 knots to avoid hard-to-explain shapes, and 3 knots are often enough to represent various biological plausible non-linear effects. Candidate models with different combinations of covariates were then developed (Table 2).

Model selection - using AIC and ten-fold cross-validation (Supplementary Table S2) - and diagnostics - using a simulation-based randomized quantile residuals and self-simulation test (see section "Detail on model diagnostic" in the online Supplementary material) - were performed to select the most parsimonious model. The most parsimonious model is the one that showed no issues with the diagnostics and had the lowest AIC and CV scores. Additionally, a jitter analysis – where starting parameter values are jittered by randomly taking samples from a normal distribution with a mean equal to the initial values (Supplementary Table S1) and a standard deviation of 0.1 – was conducted 20 times to assess the stability of the most parsimonious model. This indicated that the most parsimonious model was stable with a maximum difference in log-likelihood of less than 1e-5 and an absolute relative difference in parameter estimates of less than 0.02%.

One exception to this process is model M1 which was included in this study to mimic the design-based approach, currently used to process the age-based mackerel density by stratum and derive an overall index of abundance-at-age for use in stock assessment. The main difference between M1 and the design-based estimator would be using the Tweedie distribution in M1 which handles the extra zeros and extreme observations differently.

All models were implemented using the R-package *TMB* (Kristensen et al. 2016) and the optimization routine *nlminb* from the *stats* package in R was used to maximize the marginal likelihood by integrating out the random effect using Laplace approximation (Skaug and Fournier 2006). The *mgcv* package (Wood 2017) was used to extract the design matrix which was then used as input to the TMB model.

Table 2: The nine models tested in the current study with their name, covariate combinations (i.e., variables included in the design matrix in *Eq* 3), and ΔAIC values. Any covariate in **bold** is treated as a factor (discrete variable) and variables in plain text are treated as continuous. The expression (1|vessel) indicates that the vessel effect is considered as a random effect and acts on the intercept. The expression (1|year_strata) indicates that the year and strata variables were concatenated into a single variable and considered as a random effect. In essence, this models the interaction effect between year and strata but only considers existing interaction terms and assumes that all existing levels are normally distributed. Finally, *s(SST, k=3)* indicates that SST was modelled as a spline smoother with 3 knots.

Model name (#)	Model formula	ΔAIC
Nospatial (M1*)	**year** + **strata** + (1|**year_strata**)	13458

Base (M2)	**year** + (1|**vessel**)	969
SST (M3)	**year** + s(SST, k=3) + (1|**vessel**)	29
CHL (M4)	**year** + s(CHL, k=3) + (1|**vessel**)	918
OMLT (M5)	**year** + s(OMLT, k=3) + (1|**vessel**)	966
SST_CHL (M6)	**year** + s(SST, k=3) + s(CHL, k=3) + (1|**vessel**)	28
SST_OMLT (M7)	**year** + s(SST, k=3) + s(OMLT, k=3) + (1|**vessel**)	0
CHL_OMLT (M8)	**year** + s(CHL, k=3) + s(OMLT, k=3) + (1|**vessel**)	916
SST_CHL_OMLT (M9)	**year** + s(SST, k=3) + s(CHL, k=3) + s(OMLT, k=3) + (1|**vessel**)	1

* M1 does not include a vessel effect because some vessels only fished one stratum in specific years. In such a case, the vessel effect and the year_strata effect are not separable.

3.5. Creating predictions

Once the most parsimonious model was selected, mackerel density at age was predicted over the 11 strata of interest between 2010-2020 (Figure 2) and a few derived quantities (e.g. centre of gravity, marginal effect of variables) were calculated to explore the changes in distribution and the effect of environmental variables.

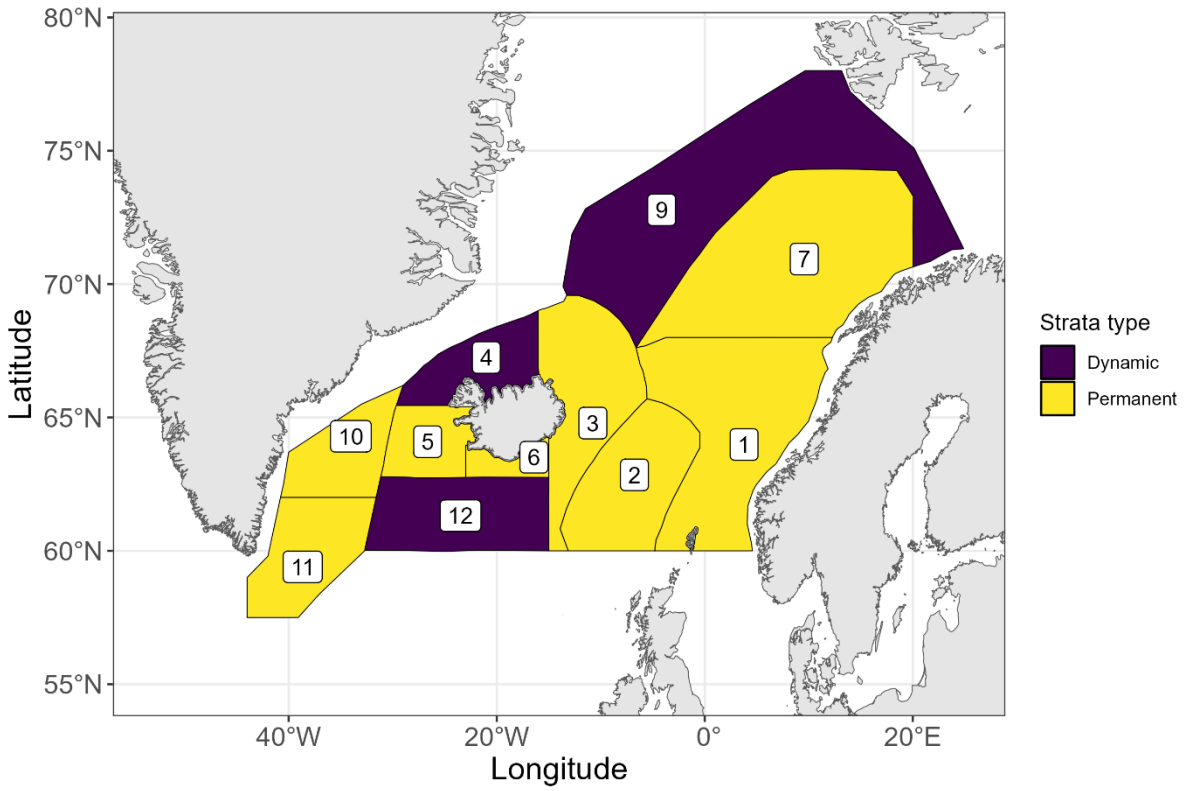

Figure 2: Mackerel IESSNS survey area and model prediction strata. Permanent stratum (yellow) and dynamics stratum (purple) are highlighted in respective colour.

3.5.1. Centre of gravity (CoG)

The CoG of the predicted mackerel density distribution was calculated to explore the overall changes in mackerel distribution over time. The annual CoGs by age and cohort were calculated through a weighted average of all cell coordinates, with the weight being the corresponding predicted mackerel density.

3.5.2. Marginal effect of environmental covariates

Marginal effect of each environmental variable – a value that reflects the effect of a variable assuming no interaction with other variables, was calculated by fixing the value of all other environmental variables to 0 (since variables were standardized, fixing them to 0 corresponds to their mean value), as well as the spatio-temporal effects to 0 (similarly, this is the mean value).

3.5.3. Total variance explained and partitioning of variance

Conditional $\mathrm{R}_{\mathrm{a}}^2$ was calculated for each candidate model and age group *a,* following the approach from Nakagawa *et al.* (2017):

$$R_a^2 = \frac{\sigma_{F,a}^2+\sigma_{w,a}^2+\sigma_{ST,a}^2}{\sigma_{F,a}^2+\sigma_{w,a}^2+\sigma_{ST,a}^2+\sigma_{resid,a}^2},\ a = 1,\ldots, A \qquad \textit{Eq 9}$$

*w*here $\sigma_{F,a}^2$ and $\sigma_{ST,a}^2$ are the empirical variance of the fixed effects and the spatio-temporal random effect for each age a, respectively. The $\sigma_{w,a}^2$ is the vessel random effect estimated by the model as defined in *Eq* 3, and

$$\sigma_{resid,a}^2 = \tau_a \overline{y_a}^{\theta_a - 2}. \qquad \textit{Eq 10}$$

where τ_a and θ_a are the tweedie distribution dispersion and power parameters as in *Eq* 8 and $\overline{y_a}$ is the mean of the data for each age group.

The contribution of individual variables to the total explained variance indicated the relative importance of the explanatory variables. The specific contribution of the environmental variable *j*, to the total explained variance for age group *a*, $\mathrm{R}_{\mathrm{j,a}}^2$, was approximated (excluding the covariance terms) as:

$$R_{j,a}^2 = \frac{var(\beta(j,a)X_j)}{var\left(\sum_{j=1}^{p}\beta_a(p)X_p\right)+\sigma_{w,a}^2+\sigma_{ST,a}^2+\sigma_{resid,a}^2} \qquad \textit{Eq 11}$$

Where $var\left(\beta(j,a)X_j\right)$ is the empirical variance of the variable *j*. Finally, the total explained variance was also partitioned in space i.e., for each IESSNS stratum, to examine differences between regions of the Nordic Seas regarding (i) the variability in the total explained variance, using *Eq* 9 and (ii) the contribution of individuals variables, using *Eq* 11. For both equations, *Eq* 9 and *Eq* 11, the calculations were limited to data points belonging to each stratum.

3.5.4. Index of abundance

The annual abundance indices for ages 3-10 equal the sum of the predictions within grids, obtained by the model described in section 2.4, across the 12 strata for each year. All grids have the same areal size. These indices reflect the overall changes in mackerel density at age over the geographic area delimited in Figure 2.

3.6. Sensitivity analysis

Previous studies using mechanistic models suggested the impact of density dependent processes leading to larger stocks occupying a larger area (Boyd *et al.*, 2020; Olafsdottir *et al.*, 2019). To explore the possible effect of density dependence, the present model was tentatively modified to include a spatially varying coefficient effect where local mackerel densities at age were allowed to change linearly with the estimated annual mackerel abundance-at-age (Thorson, 2022). For instance, if mackerel at age 5 expanded its distribution to the north and west when its abundance was higher, we would expect a positive linear effect of abundance in these areas. On the contrary, if species density is expected to decrease in the core area when abundance is high, we would expect a negative local effect in the core area.

An additional sensitivity testing was conducted to investigate the influence of mesh structure - coarser versus finer mesh - on model results (e.g. derived abundance indices, estimated spatial range) as INLA models are sensitive to spatial mesh construction (Damly *et al.* 2023).

4. Results

4.1. Overview of the model results

Model M7 was the most parsimonious model based on AIC (Table 2) and showed a reasonable fit to the data i.e. the QQ-plot did not show any misfits and simulation testing indicated no signs of overfitting or model misspecification (Supplementary Table S2 and the section “Detail on model diagnostic” in the online Supplementary material). The results presented here are based on M7; comparisons of model outputs (M2-M9) can be found in Supplementary Figures S8-9.

Model M7 explained more than 60% of the total variance in the data across age groups (Figure 3) and performed better than the non-spatial model (M1 in Table 2) in terms of diagnostics, model selection, and total amount of explained variance (Supplementary Table S2 and Supplementary Figure S8).

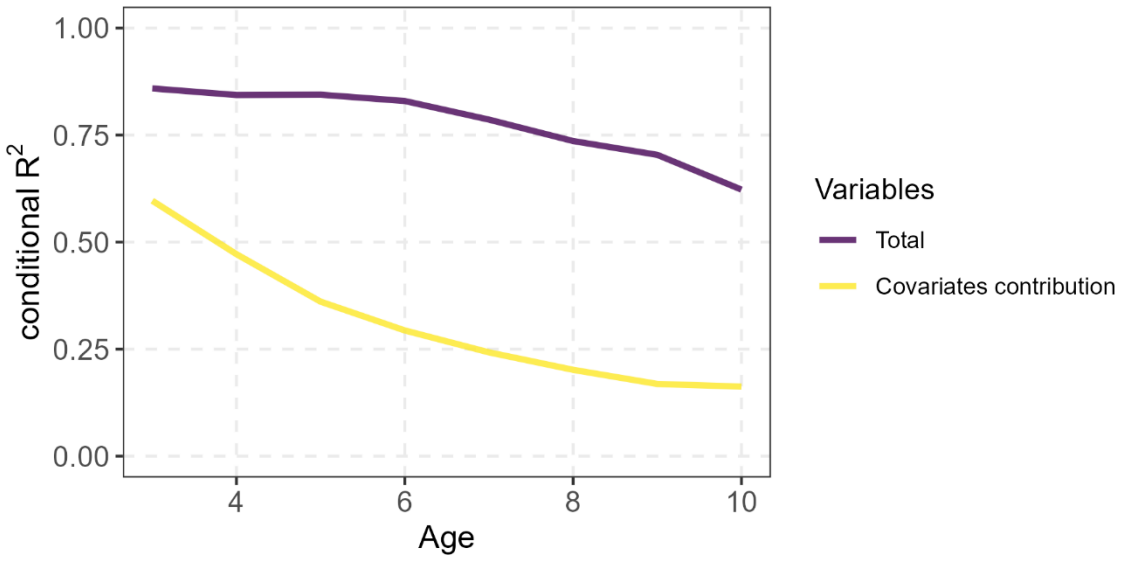

Figure 3: Total explained variance (conditional R^2) by model M7 for mackerel aged 3 – 10 and the contribution of all fixed effects in explaining the total explained variance per age.

4.2. The importance of environmental variables in explaining mackerel distribution.

SST and OMLT were more important than CHL in explaining changes in mackerel density at age over space and time as reflected by model M7. Among them, SST was the strongest contributor over all ages and showed the highest contribution to the total variance explained for ages 3-5 (Table 3 and Figure S8). The effects and importance of SST and OMLT in explaining the total variability in species distribution decreased with age (Figure 3). For example, while these variables explained a large proportion of the total R^2 for young mackerel (close to or more than 50% for ages 3 and 4), its importance decreased to less than 20% for age 10 (Figure 3). The vessel random effect only contributed to 1% of the total R^2 in model M7.

The estimated shapes of the environmental effects (seen via the marginal effect plots in Figure 4) did not qualitatively change between candidate models (Supplementary Figure S9). The SST had a dome-shaped relationship with mackerel density, with peaks around 8.5 - 12° C. Younger age groups showed a stronger response to SST showing a narrower window of favourable SST values (Figure 4a). The threshold temperature, below which conditions became unfavourable (i.e. when the marginal effect curve dropped below 0), was 7.5, 7.2, 6.2, 5.6, 5.2, 4.4°C for ages 3, 4, 5, 6, 7, and 8+ respectively.

The effect of OMLT was U-shaped for all ages with lower and higher mixed layer depth being more favourable for mackerel than average depth (Figure 4b). Moreover, none of the observed OMLT values yielded a negative effect on mackerel density (i.e. no negative values in Figure 4b).

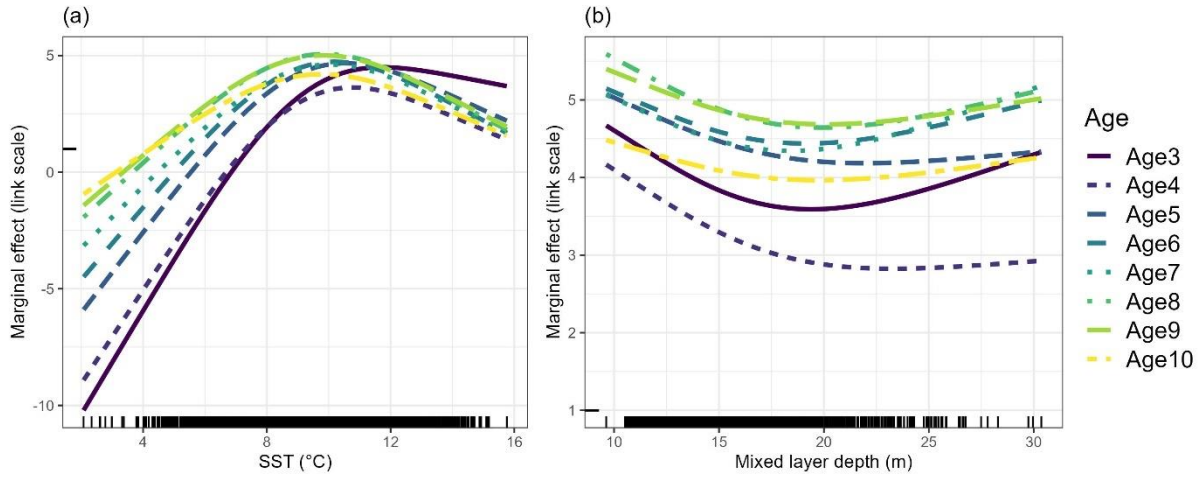

Figure 4: Marginal effect of (a) SST and (b) OMLT included in the model M7.

When examined across space, the explanatory power of environmental variables differed depending on the region. The environmental variables heavily contributed to the observed variability in strata 3, 4, and 9, regions of ocean fronts. The variables explained between 14-66% of variance depending on the age group, with greater influence on younger individuals, above 50% for ages 3-4 (Table 3). SST was the major contributor explaining as much as 61% (66 × 0.93) of the total variability for age 3 mackerel density in stratum 4 (Table 3). In the southern Norwegian Sea and closer to the "centre" of the mackerel distribution i.e., strata 1, 2, 5, 6, and 12 (Figure 3 and 5), the environmental variables only explained between 5-24% of the observed variability, a reduced proportion compared to frontal regions (Table 3). In strata 7, 10 and 11, the westernmost and northern Norwegian Sea regions, the

environmental variables explained again between 27-45% of observed variability especially for younger mackerel ages 3-4 (Table 3).

Table 3: Percentage of total variance explained by all the environmental variables together in the most parsimonious model (M7) within each IESSNS stratum (row) and mackerel age 3 – 10 (column). The numbers in parentheses indicate the percent contribution of the SST in the explained variance. Values are colour-coded in grey tone for visual aid: below 50% is coloured in light grey, above 50% in grey and bold font, and above 75% in black and bold font.

		AGE							
		3	***4***	***5***	***6***	***7***	***8***	***9***	***10***
STRATA	***1***	25% (17%)	22% (16%)	17% (24%)	15% (47%)	11% (47%)	11% (**56%**)	8% (**57%**)	10% (39%)
	2	24% (28%)	16% (16%)	12% (16%)	9% (16%)	8% (15%)	8% (18%)	5% (21%)	8% (11%)
	3	**55%** (**84%**)	49% (**82%**)	38% (**84%**)	32% (**85%**)	27% (**78%**)	22% (**76%**)	18% (**74%**)	14% (**50%**)
	4	**66%** (**93%**)	**61%** (**92%**)	**53%** (**94%**)	48% (**95%**)	39% (**92%**)	31% (**91%**)	28% (**88%**)	18% (**77%**)
	5	22% (18%)	12% (6%)	7% (6%)	5% (10%)	6% (9%)	6% (16%)	8% (12%)	10% (7%)
	6	21% (4%)	14% (2%)	10% (4%)	8% (14%)	10% (14%)	10% (20%)	10% (16%)	13% (9%)
	7	42% (50%)	27% (41%)	19% (42%)	15% (41%)	14% (33%)	12% (30%)	9% (38%)	14% (14%)
	9	**53%** (**87%**)	**51%** (**84%**)	43% (**84%**)	38% (**89%**)	34% (**86%**)	30% (**84%**)	25% (**90%**)	26% (**64%**)
	10	45% (**74%**)	28% (**77%**)	21% (**77%**)	17% (**76%**)	14% (**72%**)	9% (**69%**)	6% (**92%**)	4% (**81%**)
	11	36% (**69%**)	30% (**62%**)	21% (**63%**)	16% (**63%**)	13% (**61%**)	11% (**53%**)	6% (**86%**)	3% (**70%**)
	12	22% (23%)	14% (9%)	9% (11%)	5% (21%)	6% (22%)	6% (29%)	6% (31%)	6% (19%)

4.3. Changes in mackerel distribution at age

As mackerel became older, their centre of distribution shifted further westward and/or northward within the Nordic Seas (Figure 5, Supplementary Figure S10-12). Differences in distribution were also observed between year-classes: while some year-classes shifted their distribution westward as they became older (2012 year-class and before), others only shifted their distribution northwards (e.g. year-classes 2013 and after) (Figure 5, Supplementary Figure S12).

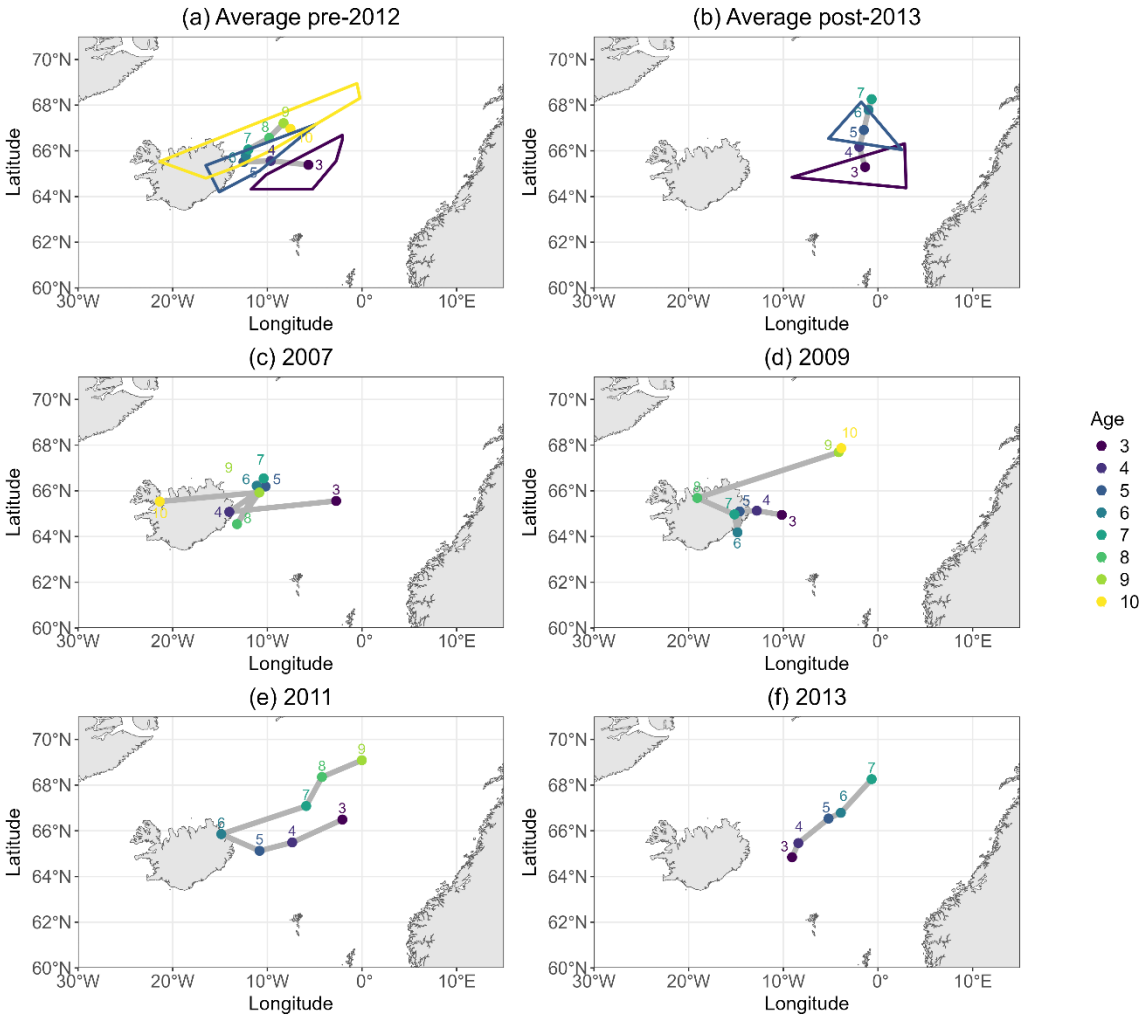

Figure 5: Changes in the CoG of selected mackerel year-classes. Panel (a) shows the average (across year-classes with equal weight between year-classes) model-derived CoG by age for mackerel pre 2012 year-classes. The contour plot illustrates the convex hull of CoG for ages 3, 5, and 10 across year-classes. Panel (b) shows the average (across year-classes with equal weight between year-classes) model-derived CoG by age for mackerel post 2013 year-classes. The contour plot illustrates the convex hull of CoG for ages 3 and 5 across year-classes. Panels (c-f) show the model-derived CoG by age for mackerel year-classes 2007, 2009, 2011, and 2013 respectively, for illustration.

4.4. Interpreting abundance indices

While there were significant differences in model fit between the candidate models (Supplementary Table S2), the abundance indices had a similar trend over time (Supplementary Figure S13-14). As expected, model M1 was most similar to the indices derived from the design-based estimator (see Supplementary Figure S13 – M1 *vs*. IESSNS). Abundance indices derived from the most parsimonious model (M7) indicated that 2010 and 2011 likely produced strong year-classes as they showed up as peaks in all indices at age (Supplementary Figure S13). However, the model was not able to perfectly track these strong year classes (2010 and 2011) over time as they fluctuated in relative importance (Supplementary Figure S14).

4.5. Sensitivity analyses

The model that included a density-dependent effect did not fit the data better than M7 and the resulting indices of abundance-at-age were similar to the model M7 (Supplementary Figure S15). Moreover, the model was not very sensitive to the mesh structure and the abundance indices at age were qualitatively the same (Supplementary Figure S16). Spatial ranges were estimated at 224, 190, and 169km for the coarse-, base-, and fine-mesh model, respectively. These spatial range estimates are a priori reasonable as they are similar but lower than those obtained for groundfish species such as cod in the Barents Sea or haddock (> 300km Breivik *et al.* in preparation).

5. Discussion

Mackerel distribution, during their summer feeding migration in Nordic Seas, appears to be influenced by both temperature and mixed layer depth, with additional spatio-temporal effects capturing the underlying variability due to unobserved variables as well as sampling effect. Previous studies showed that including both the spatio-temporal random effects and environmental covariates in the same modelling framework led to most accurate reflection of a species distribution (Brodie et al. 2021). For mackerel, temperature has been shown to be important for its distribution (Nikolioudakis et al., 2019; Olafsdottir et al., 2019). This study showed how the spatial temperature regime could influence the variability in distribution with age. Indeed, mackerel responses to temperature decreased with age and temperature influence varied between regions. The highest impact was noted in frontal regions, where cold Arctic waters were present, while the lowest in regions characterized by temperate Atlantic waters.

5.1. Thermal regimes and mackerel migration – size matters

As mackerel grow (age/size), they became more resilient to lower ambient temperatures, as evident by its expanded distribution in colder water masses, widening at the same time its thermal tolerance range. Our results show that the estimated optimal temperature for mackerel density by age decreased by approximately 3.5 °C for age 10 individuals (8.5 °C) compared to the optimal temperature for those of age 3 (~12 °C). Concomitantly, the threshold temperature – below which temperature had negative effect on mackerel density – decreased with age, being at 7.5 °C for younger fish (ages 3 and 4) and reaching as low as 4.4 °C for the older ages (ages 9 and 10). Such ontogenetic shift in fish temperature preference is well know from the literature (McCauley and Huggins, 1979; Lafrance et al., 2005) and has been related to changes in body size as optimal temperature for growth decreases with size (Freitas et al., 2010; Morita et al., 2010).

Nevertheless, are these temperature effects real or are these confounded with differential migration capability of mackerel at ages? It is well known that mackerel migratory capacity increases with age (Ono et al. 2022) as its swimming efficiency increases with size (Nøttestad et al., 1999). Therefore, younger individuals are expected to be found in areas closer to the starting point of the summer feeding migration of the species. There is no predefined boundary where the mackerel spawning migration ends and the feeding migration begins. The southern boundary of the IESSNS survey is located at latitude 60 °N on the European continental shelf. Mackerel spawn along the shelf edge as far north as 60 °N (Brunel et al., 2017). For the purpose of the current study, we assume that the feeding migration begins at latitude 60 °N and longitude 5 °W. Mackerel size distribution within the feeding area in July, measured during the IESSNS survey, shows how smaller mackerel is distributed

northward within the warmer eastern part of the Norwegian Sea (strata 1, 2, and 7) to latitudes 68 - 70 °N which is approximately 1000 km to 1250 km from the assumed migration origin (Nøttestad et al., 2010, 2011, 2012, 2013, 2014, 2015, 2016a, 2017, 2019; Olafsdottir et al., 2018; ICES, 2020). In the colder western part of the Norwegian Sea and the cold shelf areas east of Iceland (stratum 3) small mackerel is not present despite the region being located approximately 450 km from the migration origin. This lack of symmetry in young mackerel presence between cold and warm regions in relation to distance from migration origin suggests that the absence in cold frontal regions is influenced by their thermal tolerance and not their swimming capacity. However, the absence of small mackerel in strata located at the greatest distance from the assumed migration origin could be impacted by the size, thus the associated swimming efficiency of the individuals. This applies both to frontal regions (strata 4 and 9) and regions dominated by temperate Atlantic waters (5, 10 and 11). Such a confounding effect is difficult to disentangle based on field data. Nonetheless, the estimated thermal preference showed a smooth transition between age groups which made sense physiologically despite the absence of such constraint in the model.

5.2. Age-disaggregated distributions using CoG

The age disaggregated mackerel distribution, illustrated by the CoG, showed two distinct shifts during the study period. First, as mackerel become older, they migrated further westward or northward, from the migration origin, within the summer feeding area (Supplementary Figure S10). It appears that mackerel year classes hatched before 2012 tended to migrate westward with age whereas year classes from 2013 and later did not. These year classes migrated northward. Second, in the summer of 2018, the mackerel CoG shifted eastward into the Norwegian Sea from Icelandic waters, for all ages (Supplementary Figure S11). In 2019 and 2020, the CoG shifted further eastward in the Norwegian Sea. One potential explanation is social learning (Corten, 2002) in combination with the numerical dominance of large year classes (Huse *et al.*, 2002). Mackerel year classes appear to follow the same migration route every year and move further afield as they get older and become larger (Ono et al., 2022). When the 2013 year-class began migrating further from the migration origin (age 5+), they followed the older and numerically-dominant 2010-2011 year classes (age 7+) which migrated mostly northward in summer 2018. This does not explain the radical eastward shift of the CoG, for all ages, from 2018 onward. (Supplementary Figure S11). Prey availability within the feeding area did not show a substantial spatial change in 2018 compared to previous years (ICES 2020). In 2018, prey availability, measured as average mesozooplankton dry weight per region during the IESSNS in July, was higher in Icelandic waters compared to the Norwegian Sea. In fact, the highest mesozooplankton dry weight per region was in Greenlandic waters where the presence of mackerel was low (Olafsdottir et al., 2018). In the following years, 2019 and 2020, mesozooplankton dry weight was higher in the Norwegian Sea compared to Icelandic and Greenlandic waters. Other potential contributing factors include the decline in the estimated spawning stock biomass (31% from 2017 to 2020, ICES, (2023)) which could have contributed to a retraction of the distributional range (Olafsdottir et al., 2019). However, this does not explain why only the westward distribution retracted but not the northward distribution in the Norwegian Sea. It remains unclear as to why the mackerel distribution shifted eastward in summer 2018.

5.3. Other influential factor: OMLT

The OMLT had a significant but small influence on mackerel distribution. The OMLT explained only a maximum of 2% of the observed variability with a minimum effect on the mackerel distribution at intermediate ages. The OMLT reflects the depth of the surface mixed layer, thus influences the vertical distribution of mackerel within the water column. In large parts of the feeding area, mackerel presence is limited to the mixed layer as temperatures below this layer are too cold for mackerel to occur (see model predictions in areas 3-11; Nøttestad et al., 2010, 2011, 2012, 2013, 2014, 2015, 2016a, 2017, 2019; Olafsdottir et al., 2018; ICES, 2020). Hence, we hypothesize that OMLT mostly controls mackerel catchability/availability to the survey gear. However, the estimated L-shaped effect is hard-to-explain. Therefore, the estimated OMLT effect may be reflecting the influence of unmeasured but correlated variable. In general, including the OMLT in the model had hardly any effect on the estimated temperature effect (Supplementary Figure S9) nor on the derived abundance indices (Supplementary Figure S13) except improving the fit of the model to the data. Future studies on mackerel distribution should try to further investigate the utility and meaning of the OMLT variable.

5.4. Other influential factor: prey/CHL

CHL concentration at the ocean surface was included in current study as an indicator of prey availability but did not emerge as an important variable in explaining mackerel distribution by age. Previous studies on mackerel distribution during the summer feeding season showed positive impact of mesozooplankton abundance, measured during the IESSNS survey in July, on mackerel presence and abundance (Nikolioudakis et al., 2018; Olafsdottir et al., 2019). Mesozooplankton is a major prey group for mackerel (Langøy et al., 2012, Bachillier et al., 2016, Kvaavik et al.,2019). The summer distribution is a consequence of a feeding migration where individual can gain on average more than 40 % in weight during the season (Óskarsson et al., 2015). It is therefore highly likely that the spatial difference in prey availability influences mackerel distribution. A direct impact of prey availability on the mackerel distribution could not be explored in the current study as neither *in situ* measurements nor model predictions of mesozooplankton abundance (or productivity – as what is measured during surveys is the left-over abundance) exist across the whole model prediction area. Our attempt to use CHL to indicate prey availability appears to be poorly supported by *in situ* measurements (Supplementary Figure S17). This lack of correlation could explain why CHL did not emerge as a significant variable explaining the mackerel distribution.

5.5. Other influential factor: the spatio-temporal random effect

While the environmental variables explained a notable portion of the total variability in the data especially in the frontal area for younger mackerel, the portion of variance explained decreased for older age groups in the southern regions. The model still explained substantial variability in the data (as illustrated by the conditional R^2 values in Figure 3) which indicates that it was the spatio-temporal random effect that captured the rest of the variability. In biological terms, these spatio-temporal random effects represent the effect of unmeasured factors that possibly influence species distribution. Prey availability is an obvious environmental factor which could be represented by the spatio-temporal random effect especially that CHL concentration poorly represented it (see section above). In regions dominated by temperate Atlantic waters, temperature did not constrain the distribution of individuals, especially the older ones, presumably allowing flexibility to search for prey or to follow prey gradients (Broms et al., 2012). Mesozooplankton abundance is highly dynamic within the feeding area, both spatially and temporally (Nøttestad et al., 2010, 2011, 2012, 2013, 2014, 2015,

2016a, 2017, 2019; Olafsdottir et al., 2018; ICES, 2020). If prey abundance is a major contributor of these spatio-temporal random effects and older mackerel have greater capacity for searching for prey, it could explain why its importance increases whilst the influence of temperature decreases as mackerel get older and bigger.

5.6. Limits and future directions

The model derived in this study uses a correlative approach linking data to covariates and finding relationships based on user-specified assumptions. This model type is known to fail when extrapolating outside the sampling frame (and locations) where a mechanistic model (e.g. Boyd et al. 2020) might have more success. Nonetheless, if more information on environmental and biotic conditions leading to the survey period as well as the movement rate/pattern were known, we could potentially improve the predictions. Nowadays, data are increasingly being collected by a range of ocean observation systems, and distribution models that account for diffusion, advection and taxis (through the use of tagging data) have recently been developed (Thorson et al., 2021). Therefore, it might be possible to integrate movement in mackerel distribution modelling in the future. That being said, existing tagging data (i.e. pit tag and spaghetti tag) for mackerel are sparsely distributed in the region and based on recovery from the fishery (possible with a selection bias), thus would not be able to provide unbiased and detailed movement decisions over the study area. Another challenge is that mackerel movement is highly variable and migration behaviour can change between cohorts due to adopted migration routes (Ono et al., 2022), an observation that was also corroborated in this study.

Another way forward would be to complement the survey catch with another data source (e.g. acoustics) in order to consider the vertical distribution of the species, thus better handling species catchability (Monnahan et al. 2021). However, mackerel does not have a swim bladder and this hampers the use of traditional acoustic instruments (echosounders) and analysis methods to derive an acoustic estimate of species abundance. Nonetheless, there have been some trials and advances on the issue revolving around the target strength of mackerel and the conversion of acoustic signal to biomass area which might enable accurate acoustic signal processing for mackerel in the future (Korneliussen 2010, Peña et al. 2021).

With any study which is examining age related distribution patterns, there is a necessity for accurate age determination of individuals. It is known that there are uncertainties in the age reading of mackerel and this is further complicated by a number of different nations and fisheries laboratories undertaking the age reading on otoliths (ICES 2019). The ageing errors introduce an unknown level of uncertainty into the results. Efforts are made to ensure accurate age readings and the potential errors are being investigated (ICES 2019). Therefore, future research should investigate methods to account for these age-reading error in spatio-temporal models. An indirect option would be to combine the modelling framework with a spatially-explicit growth (age-length) model to take advantage of the more abundant and accurately measured length data to account for uncertainty in age estimation when converting length to ages.

5.7. Summary

We developed a spatio-temporal model of mackerel distribution, for ages 3 to 10, to investigate the age-based response of mackerel to environmental conditions and their distribution dynamics during the summer months in the Nordic Seas, between 2010-2020. Among the variables tested,

temperature was the most important one affecting mackerel distribution with older/larger individuals becoming more resilient to colder water masses and showing a wider thermal tolerance range than younger individuals, as expected by the ontogenetic changes in physiological requirement. The influence of temperature was most pronounced in the frontal regions where it was the main factor explaining the variability in mackerel density, especially for younger individuals though some of this could be confounded with the limited migration capability of young mackerels. On the other hand, in regions dominated by temperate Atlantic waters, environmental conditions explained only a small portion of the observed variability in mackerel distribution for all ages. This suggested unobserved factors, such as prey availability or currents, were likely having a larger influence on the observed distribution.

6. Acknowledgements

We are grateful to Dr Maxime Olmos and one anonymous reviewer for their thorough review which helped improve the manuscript. We also thank all the technical staff that collected the survey data.

7. Author contributions

KO contributed to all aspects of the study. All other authors contributed to the conceptualization, interpretation of the results, and editing of the manuscript.

8. Funding

This study was carried out as part of the project “Sustainable multi-species harvest from the Norwegian Sea and adjacent ecosystems” funded by the Research Council of Norway (project number 299554).

9. Data availability statement

Mackerel total catch weight, biological measurements of specimens, and information on trawling parameters from the IESSNS for the 2010 to 2020 period are available from the Planning Group on Northeast Atlantic Pelagic Ecosystem Surveys (PGNAPES) database hosted at the Faroes Marine Research Institute, Torshavn, Faroe Islands. All the code is available at https://github.com/Kotkot/MackerelST

10. Conflict of interest

The authors declare that they have no known competing financial interests or personal relationships that could have appeared to influence the work reported in this paper.

11. References

Astthorsson, O. S., Valdimarsson, H., Gudmundsdottir, A., and Óskarsson, G. J. 2012. Climate-related variations in the occurrence and distribution of mackerel (Scomber scombrus) in Icelandic waters. ICES Journal of Marine Science, 69: 1289–1297.

Bakka, H., Vanhatalo, J., Illian, J. B., Simpson, D., and Rue, H. 2019. Non-stationary Gaussian models with physical barriers. Spatial Statistics, 29: 268–288. Elsevier B.V. https://doi.org/10.1016/j.spasta.2019.01.002.

Barange, M., Coetzee, J., Takasuka, A., Hill, K., Gutierrez, M., Oozeki, Y., Lingen, C. van der, *et al.* 2009. Habitat expansion and contraction in anchovy and sardine populations. Progress in Oceanography, 83: 251–260.

625 Bachillier, E., Skaret, G., Nøttestad, L., Slotte, A., 2016. Feeding ecology of Northeast Atlantic
626 mackerel, Norwegians spring-spawning herring and blue whiting in the Norwegian Sea. PLoS One
627 11 (2), e0149238.
628 Blindheim, J. and Østerhus, S. (2005). The Nordic Seas, Main Oceanographic Features. In The Nordic
629 Seas: An Integrated Perspective (eds H. Drange, T. Dokken, T. Furevik, R. Gerdes and W.
630 Berger). https://doi.org/10.1029/158GM03
631 Boyd, Rj., Sibly, R., Hyder, K., Walker, N., Thorpe, R., and Roy, S. 2020. Simulating the summer
632 feeding distribution of Northeast Atlantic mackerel with a mechanistic individual-based model.
633 Progress in Oceanography, 183: 102299.
634 Breivik, O. N., Aanes, F., Søvik, G., Aglen, A., Mehl, S., and Johnsen, E. 2021. Predicting abundance
635 indices in areas without coverage with a latent spatio-temporal Gaussian model. ICES Journal of
636 Marine Science, 78: 2031–2042.
637 Broms, C., Melle, W., and Horne, J. K. 2012. Navigation mechanisms of herring during feeding
638 migration: the role of ecological gradients on an oceanic scale. Marine Biology Research, 8:
639 461–474. Taylor & Francis. https://doi.org/10.1080/17451000.2011.640689.
640 Carscadden, J. E., Gjøsæter, H., and Vilhjálmsson, H. 2013. A comparison of recent changes in
641 distribution of capelin (Mallotus villosus) in the Barents Sea, around Iceland and in the
642 Northwest Atlantic. Progress in Oceanography, 114: 64–83.
643 Corten, A. 2002. The role of "conservatism" in herring migrations. Review in Fish Biology and
644 Fisheries, 11: 339–361.
645 Dambly, L. I., Isaac, N. J. B., Jones, K. E., Boughey, K. L., and O'Hara, R. B. 2023. Integrated species
646 distribution models fitted in INLA are sensitive to mesh parameterisation. Ecography, e06391.
647 dos Santos Schmidt, T. C., Slotte, A., Olafsdottir, A. H., Nøttestad, L., Jansen, T., Jacobsen, J. A.,
648 Bjarnason, S., *et al.* 2024. Poleward spawning of Atlantic mackerel (*Scomber scombrus*) is
649 facilitated by ocean warming but triggered by energetic constraints. ICES Journal of Marine
650 Science, 81: 600-615.
651 Dragesund, O., Johannessen, A., and Ulltang, Ø. 1997. Varlation in migration and abundance of
652 norwegian spring spawning herring (*Clupea harengus* L.). Sarsia, 82: 97–105.
653 Frank, K. T., Carscadden, J. E., and Simon, J. E. 1996. Recent excursions of capelin (*Mallotus villosus*)
654 to the Scotian Shelf and Flemish Cap during anomalous hydrographic conditions. Canadian
655 Journal of Fisheries and Aquatic Sciences, 53: 1473–1486.
656 Freitas, V., Cardoso, J. F. M. F., Lika, K., Peck, M. A., Campos, J., Kooijman, S. A. L. M., and Veer, H. W.
657 Van Der. 2010. Temperature tolerance and energetics : a dynamic energy budget-based
658 comparison of North Atlantic marine species. Philosophical Transactions of the Royal Society B,
659 365: 3553–3565.
660 Hansen, B., and Østerhus, S. 2000. North Atlantic-Nordic Seas exchanges. Progress in Oceanography,
661 45: 109–208.
662 Hartig F (2022). DHARMa: Residual Diagnostics for Hierarchical (Multi-Level / Mixed) Regression
663 Models. R package version 0.4.6
664 Huse, G., Railsback, S., and Feronö, A. 2002. Modelling changes in migration pattern of herring:
665 collective behaviour and numerical domination. Journal of Fish Biology, 60: 571–582.
666 ICES. 2014. Report of the Benchmark Workshop on Pelagic Stocks (WKPELA).
667 ICES. 2019. Report of the Workshop on Age Estimation of Atlantic Mackerel (scomber scombrus)
668 (WKARMAC2), 22–26 October 2018, San Sebastian, Spain. ICES CM 2018/EOSG:32 . 96 pp
669 ICES. 2020. Cruise report from the International Ecosystem Summer Survey in the Nordic Seas
670 (IESSNS) 1st July – 4th August 2020.: 55 pp.
671 ICES. 2021. Cruise report from the International Ecosystem Summer Survey in the Nordic Seas
672 (IESSNS) 30th June – 3rd August 2021.

673 ICES. 2022a. Mackerel (Scomber scombrus) in subareas 1-8 and 14 and division 9.a (the Northeast
674 Atlantic and adjacent waters). In Report of the ICES Advisory Committee, 2022. ICES Advice
675 2022, mac.27.nea. https://doi.org/10.17895/ices.advice.7789
676 ICES. 2022b. Working Group on International Pelagic Surveys (WGIPS). ICES Scientific Reports. 4:82.
677 622 pp. http://doi.org/10.17895/ices.pub.20502822
678 ICES. 2023. Working Group on Widely Distributed Stocks (WGWIDE). ICES Scientific Reports. 5:82.
679 980 pp. https://doi.org/10.17895/ices.pub.24025482
680 Jansen, T., Post, S., Kristiansen, T., Óskarsson, G. J., Boje, J., MacKenzie, B. R., Broberg, M., *et al.*
681 2016. Ocean warming expands habitat of a rich natural resource and benefits a national
682 economy. Ecological Applications, 26: 2021–2032.
683 Korneliussen, R. J. 2010. The acoustic identification of Atlantic mackerel. ICES Journal of Marine
684 Science, 67: 1749–1758.
685 Kraskura, K., Hardison, E. A., and Eliason, E. J. 2023. Body size and temperature affect metabolic and
686 cardiac thermal tolerance in fish. Scientific Reports, 13: 1–16. Nature Publishing Group UK.
687 https://doi.org/10.1038/s41598-023-44574-w.
688 Kristensen, K., Nielsen, A., Berg, C. W., Skaug, H., and Bell, B. 2016. TMB: automatic differentiation
689 and laplace approximation. Journal of Statistical Software, 70: 1–21.
690 Kvaavik C, Óskarsson GJ, Daníelsdóttir AK, Marteinsdóttir G. 2019. Diet and feeding strategy of
691 Northeast Atlantic mackerel (Scombrus scomber) in Icelandic waters. PLoS One.
692 14(12):e0225552.
693 Kvamme, C., Nøttestad, L., Fernö, A., Misund, O., Dommasnes, A., Axelsen, B., Dalpadado, P., *et al.*
694 2003. Migration patterns in Norwegian spring-spawning herring: why young fish swim away from
695 the wintering area in late summer. Marine Ecology Progress Series, 247: 197–210.
696 Lafrance, P., Castonguay, M., Chabot, D., and Audet, C. 2005. Ontogenetic changes in temperature
697 preference of Atlantic cod. Journal of Fish Biology (2005) 66, 553–567. doi:10.1111/j.1095-
698 8649.2005.00623.x
699 Langøy, H., Nøttestad, L., Skaret, G., Broms, C., Fernö, A., 2012. Overlap in distribution and diets of
700 Atlantic mackerel (Scomber scombrus), Norwegian spring-spawning herring (Clupea harengus)
701 and blue whiting Micromesistius poutassou) in the Norwegian Sea during late summer. Mar.
702 Biol. Res. 8, 442–460.
703 Lindgren, F., Rue, H., and Lindström, J. 2011. An explicit link between Gaussian fields and Gaussian
704 Markov random fields: The SPDE approach. Journal of the Royal Statistical Society Series B, 73:
705 423–498.
706 McCauley, R.W. And Huggins, N.W. 1979. Ontogenetic and non-thermal seasonal effects on thermal
707 preferenda of fish. American Zoologist, 19: 267-271.
708 Monnahan, C. C., Thorson, J. T., Kotwicki, S., Lauffenburger, N., Ianelli, J. N., and Punt, A. E. 2021.
709 Incorporating vertical distribution in index standardization accounts for spatiotemporal
710 availability to acoustic and bottom trawl gear for semi-pelagic species. ICES Journal of Marine
711 Science, 78: 1826–1839.
712 Morita, K., Fukuwaka, M. aki, Tanimata, N., and Yamamura, O. 2010. Size-dependent thermal
713 preferences in a pelagic fish. Oikos, 119: 1265–1272.
714 Nielsen, A., and Berg, C. W. 2014. Estimation of time-varying selectivity in stock assessments using
715 state-space models. Fisheries Research, 158: 96–101. Elsevier B.V.
716 http://dx.doi.org/10.1016/j.fishres.2014.01.014.
717 Nikolioudakis, N., Skaug, H. J., Olafsdottir, A. H., Jansen, T., Jacobsen, J. A., and Enberg, K. 2019.
718 Drivers of the summer-distribution of Northeast Atlantic mackerel (*Scomber scombrus*) in the
719 Nordic Seas from 2011 to 2017; a Bayesian hierarchical modelling approach. ICES Journal of
720 Marine Science, 76: 530–548.

Nøttestad, L., Giske, J., Holst, J. C., and Huse, G. 1999. A length-based hypothesis for feeding migrations in pelagic fish, 56.

Nøttestad, L., Jacobsen, J.A., Sveinbjornsson, S., 2010. Cruise Report from the Coordinated Ecosystem Survey with M/VLibas, M/V Brennholm, M/V Finnur Fridi and R/VArni Fridriksson in the Norwegian Sea and Surrounding Waters, 9 July–20 August 2010. Working Document to Working Group of Widely Distributed Stocks, ICES, Copenhagen, Denmark, 28 August–3 September 2010.

Nøttestad, L., Holst, J.C., Utne, K.R., Tangen, Ø., Anthonypillai, A., Skalevik, A., Mork, K. A., et al., 2011. Cruise Report from the Coordinated Ecosystem Survey (IESSNS) with M/VLibas, M/V Finnur Fridi and R/VArni Fridriksson in the Norwegian Sea and Surrounding Waters, 18 July–31 August 2011. Working Document to Working Group of Widely Distributed Stocks, ICES, Copenhagen, Denmark, 27 August–2 September 2011.

Nøttestad, L., Utne, K.R., Anthonypillai, V., Tangen, Ø., Valdemarsen, J.W., Oskarsson, G., Sveinbjornsson, S., et al., 2012. Cruise Report from the Coordinated Ecosystem Survey (IESSNS) with R/V G.O. Sars, M/V Brennholm, M/V Christian í Grótinum and R/VArni Fridriksson in the Norwegian Sea and surrounding waters, 1 July–10 August 2012. Working Document to Working Group of Widely Distributed Stocks, ICES, Lowestoft, UK, 21–27 August 2012.

Nøttestad, L., Utne, K.R., Anthonypillai, V., Tangen, Ø., Valdemarsen, J.W., Oskarsson, G., Sveinbjornsson, S., et al., 2013. Cruise Report from the Coordinated Ecosystem Survey (IESSNS) with M/V Libas, M/V Eros, M/V Finnur Fríði and R/V Arni Fridriksson in the Norwegian Sea and surrounding waters, 2 July–9 August 2013. Working Document to Working Group of Widely Distributed Stocks, ICES, Copenhagen, Denmark, 27 August–2 September 2013.

Nøttestad, L., Salthaug, A., Johansen, G.O., Anthonypillai, V., Tangen, Ø., Utne, K.R., Sveinbjornsson, S., et al., 2014. Cruise Report from the Coordinated Ecosystem Survey (IESSNS) with M/V Brennholm, M/V Vendla, M/V Finnur Fríði and R/Varni Fridriksson in the Norwegian Sea and surrounding waters, 2 July–12 August 2014. Working Document to Working Group of Widely Distributed Stocks, ICES, Copenhagen, Denmark, 26 August–1 September 2014.

Nøttestad, L., Anthonypillai, V., Tangen, Ø., Utne, K. R., Óskarsson, G. J., and Jónsson, S. Þ. 2015. Cruise report from the International Ecosystem Summer Survey in the Nordic Seas (IESSNS) with M/V ”Brennholm”, M/V “Eros”, M/V “Christian í Grótinum” and R/V “Árni Friðriksson”, 1 July - 10 August 2015.

Nøttestad, L., Utne, K. R., Óskarsson, G. J., Jónsson, S. Þ., Jacobsen, J. A., Tangen, Ø., Anthonypillai, V., *et al.* 2016a. Quantifying changes in abundance, biomass, and spatial distribution of Northeast Atlantic mackerel (*Scomber scombrus*) in the Nordic seas from 2007 to 2014. ICES Journal of Marine Science: Journal du Conseil, 73: 359–373.

Nøttestad, L., Anthonypillai, V., Tangen, Ø., Høines, Å., Utne, K. R., Óskarsson, G. J., Ólafsdóttir, A. H., *et al.* 2016b. Cruise report from the International Ecosystem Summer Survey in the Nordic Seas (IESSNS) with M/V ”M. Ytterstad”, M/V “Vendla”, M/V “Tróndur í Gøtu”, M/V “Finnur Fríði” and R/V “Árni Friðriksson”, 1 – 31 July 2016.

Nøttestad, L., Anthonypillai, V., Høines, Å., Salthaug, A., Utne, K. R., Ólafsdóttir, A. H., and Jónsson, S. Þ. 2017. Cruise report from the International Ecosystem Summer Survey in the Nordic Seas (IESSNS) with M/V ”Kings Bay”, M/V “Vendla”, M/V “Tróndur í Gøtu”, M/V “Finnur Fríði” and R/V “Árni Friðriksson”, 3rd of July – 4th of August 2017.

Nøttestad, L., Anthonypillai, V., Vatnehol, S., Salthaug, A., Høines, Å., Ólafsdóttir, A. H., Homrum, E., et al. 2020. Cruise report from the International Ecosystem Summer Survey in the Nordic Seas (IESSNS) 28th June - 5th August 2019: 1–60.

Ólafsdóttir, A. H., Jónsson, S. Þ., Kennedy, J., Jacobsen, J. A., Mortensen, E., Smith, L., Jansen, T., et al. 2018. Cruise report from the International Ecosystem Summer Survey in the Nordic Seas (IESSNS) 30th of June – 6th of August 2018.

Olafsdottir, A. H., Utne, K. R., Jacobsen, J. A., Jansen, T., Óskarsson, G. J., Nøttestad, L., Elvarsson, B. Þ., *et al.* 2019. Geographical expansion of Northeast Atlantic mackerel (Scomber scombrus) in the Nordic Seas from 2007 to 2016 was primarily driven by stock size and constrained by low temperatures. Deep Sea Research Part II: Topical Studies in Oceanography, 159: 152–168.

Ólafsdóttir, A. H., Jónsson, S. Þ., Kennedy, J., Jacobsen, J. A., Mortensen, E., Smith, L., Jansen, T., *et al.* 2018. Cruise report from the International Ecosystem Summer Survey in the Nordic Seas (IESSNS) 30th of June – 6th of August 2018.

Ono, K., Slotte, A., Hølleland, S., Mackinson, S., Jónsson, S. Þ., Jacobsen, J. A., and Ólafsdóttir, A. H. 2022. Space-time recapture dynamics of PIT-tagged Northeast Atlantic mackerel (Scomber scombrus) reveal size-dependent migratory behaviour. Frontiers in Marine Science, 9: 983962.

Óskarsson, G. J., Gudmundsdottir, A., Sveinbjörnsson, S., and Sigurðsson, Þ. 2016. Feeding ecology of mackerel and dietary overlap with herring in Icelandic waters. Marine Biology Research, 12: 16–29.

Peña, H., Macaulay, G. J., Ona, E., Vatnehol, S., and Holmin, A. J. 2021. Estimating individual fish school biomass using digital omnidirectional sonars, applied to mackerel and herring. ICES Journal of Marine Science, 78: 940–951.

Read, J. F., and Pollard, R. T. 1992. Water masses in the region of the Iceland-Faroes front. Journal of physical oceanography, 22: 1365–1378.

Roy, C., van der Lingen, C., Coetzee, J., and Lutjeharms, J. 2007. Abrupt environmental shift associated with changes in the distribution of Cape anchovy *Engraulis encrasicolus* spawners in the southern Benguela. African Journal of Marine Science, 29: 309–319.

Skaug, H. J., and Fournier, D. A. 2006. Automatic approximation of the marginal likelihood in non-Gaussian hierarchical models. Computational Statistics and Data Analysis, 51: 699–709.

Stefánsson, U., and Ólafsson, J. 1991. Nutrients and fertility of Icelandic waters. Rit Fiskideildar, 7: 1–56.

Thorson, J. T. 2019. Guidance for decisions using the Vector Autoregressive Spatio-Temporal (VAST) package in stock, ecosystem, habitat and climate assessments. Fisheries Research, 210: 143–161.

Thorson, J. T., Barbeaux, S. J., Goethel, D. R., Kearney, K. A., Laman, E. A., Nielsen, J. K., Siskey, M. R., *et al.* 2021. Estimating fine-scale movement rates and habitat preferences using multiple data sources. Fish and Fisheries, 22: 1359–1376.

Thorson, J. T. 2022. Development and simulation testing for a new approach to density dependence in species distribution models. ICES Journal of Marine Science, 79: 117–128.

Trenkel, V. M., Huse, G., MacKenzie, B. R., Alvarez, P., Arrizabalaga, H., Castonguay, M., Goñi, N., *et al.* 2014. Comparative ecology of widely distributed pelagic fish species in the North Atlantic: Implications for modelling climate and fisheries impacts. Progress in Oceanography, 129: 219–243.

Turrell, B. 1995. A century of hydrographic observations in the Faroe–Shetland Channel. Ocean Challenge, 6: 58–63

Utne, K. R., Huse, G., Ottersen, G., Holst, J. C., Zabavnikov, V., Jacobsen, J. A., Óskarsson, G. J., *et al.* 2012. Horizontal distribution and overlap of planktivorous fish stocks in the Norwegian Sea during summers 1995–2006. Marine Biology Research, 8: 420–441.

Wood, S.N. 2003. Thin-plate regression splines. Journal of the Royal Statistical Society (B) 65(1):95-114.

Wood, S.N. 2011. Fast stable restricted maximum likelihood and marginal likelihood estimation of semiparametric generalized linear models. Journal of the Royal Statistical Society (B) 73(1):3-36